ELSEVIER

Journal of Photochemistry and Photobiology A: Chemistry 122 (1999) 175–183

Journal of Photochemistry and Photobiology A:Chemistry

The effect of selected reaction parameters on the photoproduction of oxygen and hydrogen from a WO_3–Fe^{2+}–Fe^{3+} aqueous suspension

Gratian R. Bamwenda, Kazuhiro Sayama, Hironori Arakawa*

National Institute of Materials and Chemical Research, 1-1 Higashi, Tsukuba, Ibaraki 305-8565, Japan

Received 26 October 1998; received in revised form 21 January 1999; accepted 22 January 1999

Abstract

The photoproduction of oxygen and hydrogen from an aqueous suspension containing WO_3, Fe^{2+}, and Fe^{3+} species was studied and a comparison of product yields made between the inner- and outer-irradiation systems. Prolonged irradiation of the WO_3–H_2O–Fe^{2+}/Fe^{3+} system led to the generation of O_2 and H_2, and the yields could be sustained for a period of several days. The product yields showed a dependence on the duration of irradiation, illumination wavelength, WO_3 concentration, concentration of Fe^{3+} and Fe^{2+} cations, type of iron (III) salt, and pH. The optimum photoproduction for O_2 and H_2 was obtained under the following operating conditions: [WO_3]: 8 g dm^{-3}, [Fe^{3+}]: 14–20 mol dm^{-3}, pH 1.5–2.5, and illumination wavelength: 200–500 nm. The illumination time needed to reach the stationary state was ca. 6 and 30 h for the inner- and outer-irradiation systems, respectively. In addition to these conditions, a ratio of [Fe^{2+}] : [Fe^{3+}] = 2–4 was found to be suitable for the simultaneous production of O_2 and H_2. The product yields from the annular photoreactor were usually about four times more than those from an outer-irradiation photoreactor. When $Fe_2(SO_4)_3$ was replaced by $Fe(NO_3)_3$ or $FeCl_3$ as a source of Fe^{3+} species, higher initial O_2 evolution rates were obtained but the long term yields were lower than those from dispersions containing $Fe_2(SO_4)_3$. The studied system utilized WO_3 to accomplish the initial light absorption, charge separation and O_2 evolution in the presence of $Fe^{2+}{}_{aq}$species as an electron acceptor, and then relied on the $Fe^{2+}{}_{aq}$ photochemical process to produce hydrogen. The overall reaction was photodecomposition of water into O_2 and H_2. Mechanistic implications were considered to account for the probable reaction steps leading to the products observed and the dependence of the yields on the examined reaction parameters.

Keywords: Photocatalysts; Tungsten trioxide; Ferrous and ferric ions; Oxygen; Hydrogen

1. Introduction

The photocatalytic production of hydrogen and oxygen from aqueous suspensions is a subject of great interest from both theoretical and practical points of view due to its possible application for converting and storing the abundant sunlight energy as chemical energy. This concept of sunlight-induced photo-splitting of water has stimulated a large amount of research leading to the development of a number of potential catalysts, and a number of encouraging results have appeared in the recent literature on this subject [1,2].

The present challenge is not only to find photocatalytic systems that can produce H_2 and O_2 from water, but also systems having long-term stability under illumination and in a variety of aqueous suspensions. Most of the photocatalytic systems studied recently include materials such as modified TiO_2 and titanates [3–8], ZrO_2 [9], tantalates [10], perovskites [11], pillared structures, e.g., $K_3Ta_3Si_2O_{13}$ [12], Cu_2O [13], and niobates [14,15].

In our group, we took a slightly different and novel approach. In order to decompose water simultaneously into H_2 and O_2, we developed a configuration that can first produce oxygen in reasonable quantities, and in the second step produce hydrogen in the same semiconductor/aqueous suspension. After preliminary tests, we found that WO_3 can allow the accomplishment of such a system [16].

Tungsten trioxide has attracted the interest of many workers because of its semiconducting nature and electrochromic properties [17]. As shown in Table 1 and Fig. 1(a), WO_3 is a material with a band gap, $E_{BG} = \sim 2.6$–3 eV, that falls within the solar spectrum and whose physicochemical properties make it attractive for photocatalysis research [18–20]. An early attempt to produce H_2 from a water–ethanol solution using WO_3 was made by Scaife [18] but without success. This was so because of the unfavorable energetics, i.e., the conduction band of WO_3 ($E_{CB} = +0.4$ V versus NHE at pH 0) is lower than the energy in $E^0_{H^+/H^2} = 0.0$ V versus NHE.

*Corresponding author. Tel.: +81-298-54-4760; fax: +81-298-54-4750.

1010-6030/99/$ – see front matter
PII: S1010-6030(99)00026-X

Table 1
Selected physicochemical properties of tungsten trioxide

Property	Value	Literature
Color [a]	yellow-greenish	tw
Density	7.3 g cm^{-3}	
Surface area	~2 m^2 g^{-1}	tw
Oxide : Metal volume ratio	3.3	[21]
Acidity, $H_{0\ max}$ [b]	1.3	[22]
$-\Delta H^0_{298}$	201 kcal mol^{-1}	[21]
$T_{melting}$	1746 K	[23]
Crystal structure [c]	monoclinic at 298 K	[23]
Refractive index	1.5 ~ 2.1	[24]
Absorption edge	~480 nm	tw
Bandgap [d]	~2.6 eV	tw
$E_{Flat\ band}$ [e]	+0.5 V	[39]
$E_{Conduction\ band}$ [e]	+0.4 V	
$E_{Valence\ band}$ [e]	+3.1 V	
Conductivity	0.1 ~ 0.5 S cm^{-1}	[40]
$E_{overvolatage}$ for O_2 evolved at pH 1	~0.8 V	[41]

[a] The greenish coloration in WO_3 indicates oxygen deficiency.
[b] Acidic strength $H_0 = pK_{BH^+}$.
[c] It is orthorombic and tetragonal at $T = 973$ and $T > 973$ K, respectively.
[d] The bandgap was estimated from the UV–Vis absorption vs. λ spectrum in Fig. 1 (a) and using the equation: $E_{BG} = 1240/\lambda_{onset}$. The bandgap given in the literature is between 2.7–2.8 eV [32,39].
[e] Potential vs. NHE at pH 0.
tw: This work.

Thus the photoexcited conduction-band electrons in WO_3 cannot reduce protons to hydrogen. On the other hand, the holes in the valence band are energetically favorably situated to oxidize water to oxygen (see Table 1). To overcome the above hindrance, we designed a combined system in which O_2 can be produced photocatalytically, e.g., over WO_3, while H_2 is generated simultaneously from a photochemical process in the same suspension. To achieve this, we used a Fe^{2+}/Fe^{3+} redox couple [16].

Usage of a Fe^{2+}/Fe^{3+} redox couple in chemical reactions is not new. Fenton [25] used ferrous ions and H_2O_2 to form hydroxyl radicals which are widely used as oxidizing agents in a variety of reactions, especially in oxidizing organic chemicals and in waste water treatment. The Fe^{2+}/Fe^{3+} redox couple has also found applications in various photochemical processes [16,19,26–30].

In this work, we report the photocatalytic activity and the effect of parameters, e.g., time dependence, long-term irradiation, pH, illumination wavelength, and concentration of Fe^{3+} and Fe^{2+} cations on the production of O_2 and H_2 from the WO_3–H_2O–$Fe^{2+}/Fe^{3+} + h\nu$ system. This work represents the second step of a systematic investigation of WO_3-based photocatalysts in the photocatalytic splitting of water.

2. Experimental

2.1. Materials

High purity powdered WO_3 (>99.9% purity) was obtained from Kojundo Chemical Co. The BET surface area of the

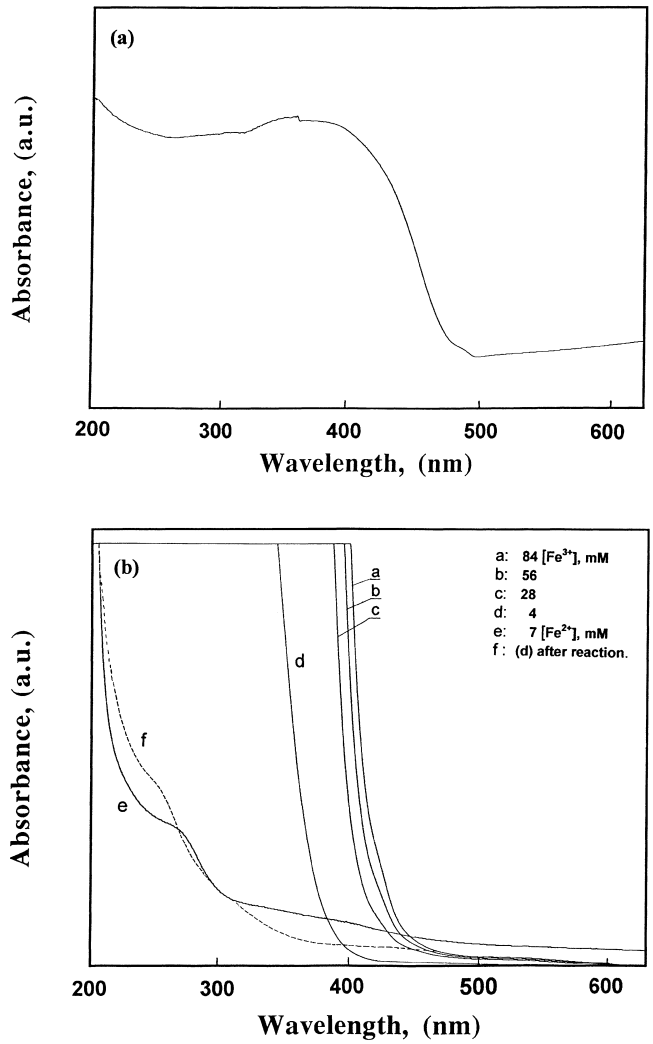

Fig. 1. UV–Vis diffuse reflectance spectra of (a) WO_3 powder and (b) aqueous solutions of iron (III) sulfate and iron (II) sulfate.

powder measured by nitrogen adsorption was ~2 m^2 g^{-1}. Solutions of Fe^{3+} and Fe^{2+} cations were made by dissolving $Fe_2(SO_4)_3 \cdot nH_2O$ (Kokusan Chemical Co.) and $FeSO_4 \cdot 7H_2O$ (99.5%, Wako Chemical Co.) in water. Ferric sulfate contained small amounts of an iron (II) salt ~0.03%. The main anion impurities in these salts were nitrates (0.01%) and chlorides (0.003%). The NaOH and H_2SO_4 acid (Wako Chemical Co.) were of analytical grade and were used as supplied. $Fe(NO_3)_3 \cdot 9H_2O$ (Kanto Chemical Co.) and $FeCl_3 \cdot 6H_2O$ (Kokusan Chemical Co.) were used as received.

2.2. Apparatus and procedures

WO_3 (0.4–3.2 g) was dispersed in 90 cm^3 of distilled, deionized water by ultrasonic agitation for 30 min. Following sonication, required amounts of Fe^{3+} and/or Fe^{2+} aqueous solutions were added so that the final volume was about 100 and 350–400 cm^3 for the outer- and inner-irradiation photoreactors, respectively. The suspension was then transferred to the reactor which was then mounted on a closed

gas-circulation system (~215 cm^{-3}), equipped with outlets to a vacuum line and GC.

Experiments were performed in two types of reactors: outer-irradiation type photoreactor, i.e., a Pyrex cell (light reaching the suspension has $\lambda_i \geq 300$ nm) having a flat window for illumination with a capacity of ~215 cm^3. In this case, the irradiation of the suspension was carried out from outside the reactor by a 500 W xenon lamp (Ushio UXL 500D) with an incident flux of 560 mW cm^{-2}, as measured with an Eppley Lab. radiometer. The second cell was an annular (inner-irradiation type) photoreactor in which irradiation from a 400 W high pressure mercury lamp (Riko Kagaku) was transverse. In this setup, light was transmitted through a Pyrex or quartz glass water jacket which was immersed vertically in a 1.1 dm^3 Pyrex glass cylinder (Ø = 75 mm) containing a 350–400 cm^3 dispersion.

Prior to illumination, the mixture was evacuated up to ~2 kPa under magnetic stirring to remove physisorbed gases. After a 2 h deaeration, that is when almost no O_2 was detected by on-line GC, small amounts of argon were added to the system and the experiment was started by illuminating the suspension under continuous stirring at an initial pressure of between 4 to 7 kPa. The course of the reaction was monitored by periodic sampling of the gas phase. The average reaction temperature was 300 and 311 ± 2 K for the inner- and outer-irradiation systems, respectively.

2.3. Analyses

Hydrogen and oxygen were analyzed by gas chromatography (Shimadzu GC-8A) equipped with a thermal conductivity detector (TCD) and a stainless steel column (2 m) packed with molecular sieves (5 Å) at 318 K. Argon was used as a carrier gas. Several reproducibility tests were performed over a range of various irradiation times. The uncertainty in the measurement of H_2 and O_2 yields was found to be less than 5% in the majority of experiments, which was adequate for the purpose of the present investigation.

3. Results

3.1. Absorption spectra

Fig. 1 shows a series of absorption spectra acquired for WO_3 powders (Fig. 1(a)) and those acquired for aqueous solutions of $FeSO_4$ and $Fe_2(SO_4)_3$ (Fig. 1(b)). The spectra clearly document that WO_3 has intense absorption in the UV–Vis region of the spectrum. The onset of absorption of WO_3 was at ~480 nm, which corresponds to the band gap energy of ca. 2.6 eV, as estimated from Eq. (1)[1].

$$E_{BG} = \frac{1240}{\lambda_{absorp.edge}} \quad (1)$$

This value is consistent with the characteristic values given in literature for WO_3 materials, i.e., ($E_{BG}^{WO_3} = 2.7$–3 eV) [32,39]. As seen in Fig. 1(b), $FeSO_4$ and $Fe_2(SO_4)_3$ solutions strongly absorb in the UV region and weakly absorb in the visible region. Ferrous sulfate solutions had a broad absorption peak at ~235 nm and absorption tailed into the near UV region. The $Fe_2(SO_4)_3$ solutions had much greater absorption in the near UV than those of $FeSO_4$, indicating that in this region, Fe^{3+} ions have a greater absorption coefficient than Fe^{2+} species. The results reported in Fig. 1 lead us to suppose that in Fe^{3+} dilute aqueous solutions, $[Fe^{3+}] \leq 5$ mM, and at $\lambda_i > 400$ nm, the solution phase will not interfere significantly with the absorption by WO_3 particles.

3.2. Photocatalytic production of oxygen

3.2.1. Time dependence, effect of long-term irradiation and pH

Tungsten trioxide exhibits weak acidic properties. As we will see below, it is fairly stable against corrosion even in strong acidic aqueous suspensions. The only drawback is that it undergoes dissolution in strongly alkaline solutions at pH > 9. The suspension obtained after dispersing WO_3 in water (4–32 g dm^{-3} WO_3) had a pH = ~4.5. Addition of ferric salts to the suspension resulted in the drop in pH to about pH 2.5, with some of the Fe^{3+} ions being transformed into $FeOH^{2+}$ according to Eq. (2).

$$Fe_{aq}^{3+} + H_2O \rightleftarrows FeOH^{2+} + H^+ \quad (2)$$

In initial oxygen production studies presented in Figs. 2, 3 and 4, we used dispersions containing low concentrations of Fe^{3+} ions and an outer-irradiation system under moderate illumination with a xenon lamp and a 420 nm sharp cut filter so as to minimize the effects of solution photochemistry.

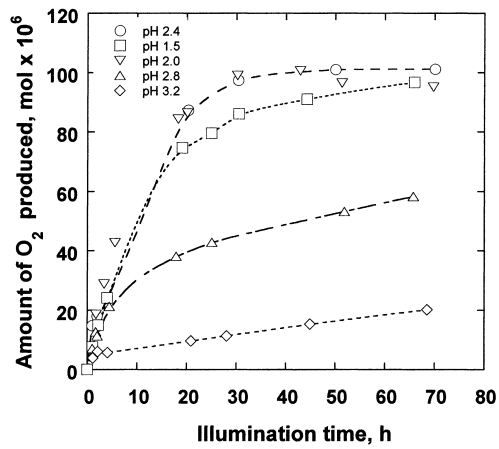

Fig. 2. Time course of oxygen evolution as a function of the pH of the suspension. Conditions: Reactor, 215 cm^3 outer-irradiation cell; light source, 500 Xe lamp; incident flux, 560 mW cm^{-2}; $\lambda_i \geq 420$ nm; T, 311 K; C_{WO_3}, 4 g dm^{-3}; $[Fe^{3+}] = 4$ mM.

Fig. 2 illustrates the time-dependence profiles and long-term photoproduction of O_2 from a 100 cm^3 aqueous WO_3–$Fe_2(SO_4)_3$ suspension containing 4 g dm^{-3} WO_3 and ca. 4×10^{-3} mol dm^{-3} Fe^{3+} at various initial pH values. Oxygen evolution was not observed in a 25 h experiment in the dark. Upon irradiation of the suspension, oxygen evolved and its yield increased progressively with reaction time (t_i) in the first 20 h and approached a plateau at $t_i > 30$ h. The main reason for such a behavior is the depletion of Fe^{3+} species, the electron acceptor, from the solution phase. As we will see further in the text, the time taken to reach the plateau depends on the initial concentration of Fe^{3+} species, and the illumination geometry. The amounts of O_2 at the plateau will be termed here as the maximum oxygen yield, n_{O_2max}. This value was retained even after 70 h of irradiation in the examined pH range.

Also shown in Fig. 2 is the relationship between O_2 yield and pH. As the pH was lowered with respect to normal pH 2.5, there were no substantial changes in the reaction profiles but O_2 yield decreased steadily with decreasing pH. At pH > 2.5, O_2 yield decreased substantially. At pH > 3.5, precipitation of Fe^{3+} occurred, resulting in much lower O_2 yields. At the end of the experiments, the final pH of the suspensions did not vary substantially from the initial values, i.e., ±0.1–0.2.

Based on the above findings, we deduce that: first, the investigated system exhibits a consistent long-term activity toward O_2 production, lasting even a couple of days; secondly, for the photoproduction of O_2 using Fe^{3+} cations as electron acceptors, the working range must lie in acidic conditions, pH < 3. From the results in Fig. 2, a pH between 1.5 and 2.5 appears to be a suitable choice for the efficient production of O_2 in the WO_3–H_2O–Fe^{3+}–$h\nu$ system. Since WO_3–H_2O–Fe^{3+} suspensions normally had a pH = ~2.5, no pH adjustments were made in later experiments. In addition to O_2, small amounts of H_2 (0.1–0.2 μmol) were also produced. It seems probable that the observed H_2 originates from either the irradiation of the solution phase or from organic impurities. But in the latter case, we could have observed carbon dioxide in the products. We couldn't because maybe it remained in the suspension or it was too minute to be detected by our present analytical procedures.

3.2.2. Effect of initial Fe^{3+} concentration

Fig. 3 shows the dependence of O_2 photogeneration on initial Fe^{3+} concentration. It is seen that the production of O_2 increased gradually as the concentration of Fe^{3+} cations was increased, and it reached the optimum in the region $[Fe^{3+}] = 14$–20 mM. Consequently, it decreased as the concentration of Fe^{3+} increased beyond the optimum value.

In view of the results presented in Figs. 1 and 3, we decided to work with low Fe^{3+} ion concentration (4×10^{-3} mol dm^{-3}) so as to minimize diffusion effects at the inter-phase layer between the WO_3 particle and the bulk of the solution. Another reason was to keep the light absorption by the solution phase to the minimum, and to avoid the inner filter effect (see Fig. 1(b)).

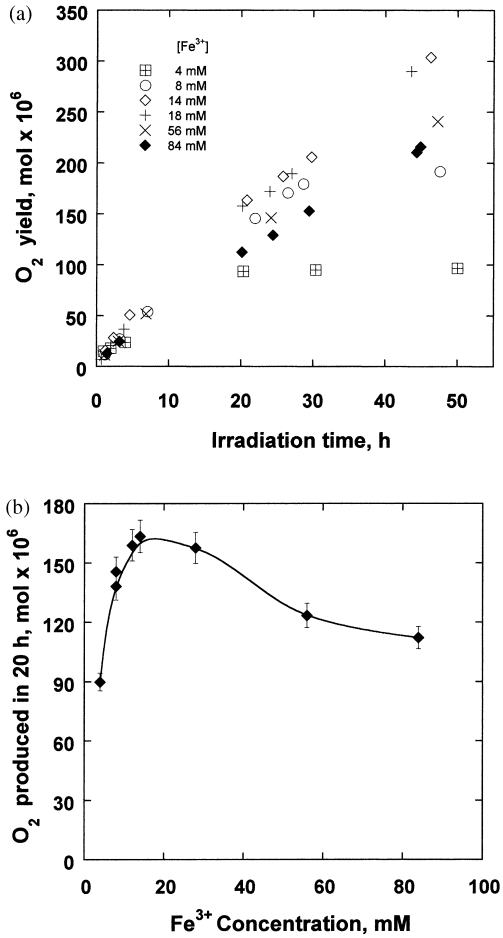

Fig. 3. Influence of Fe^{3+} concentration on the yield of O_2 obtained with 4 g dm^{-3} WO_3 dispersed in 100 cm^3 aqueous solutions. pH = 2.4 ~ 2.5. Other conditions as in Fig. 2.

3.2.3. Influence of WO_3 concentration

The variation in O_2 yield as a function of the amount of WO_3 in the suspension (C_{WO_3}), at an initial concentration of 4×10^{-3} mol dm^{-3} Fe^{3+} and at pH 2.4, is displayed in Fig. 4. At small WO_3 concentrations, O_2 yield increased in proportion to the WO_3 content in the suspension, passing through a weak maximum at about $C_{WO_3} = \sim 8$ g dm^{-3}, which was reproduced in three repeat runs with a deviation of ~3%. Above this value, O_2 yield was more or less independent of the amount of WO_3 used. This result indicates that the 8 g dm^{-3} WO_3 suspension facilitates the most efficient light absorption, and/or that the saturation of the suspension by photons is reached at this concentration. In the light of these results, the concentration of WO_3 was fixed at 8 g dm^{-3} in later experiments.

3.2.4. Effect of illumination wavelength and type of iron (III) salt

To explore the influence of illumination wavelength range on O_2 evolution activity, runs were conducted using appro-

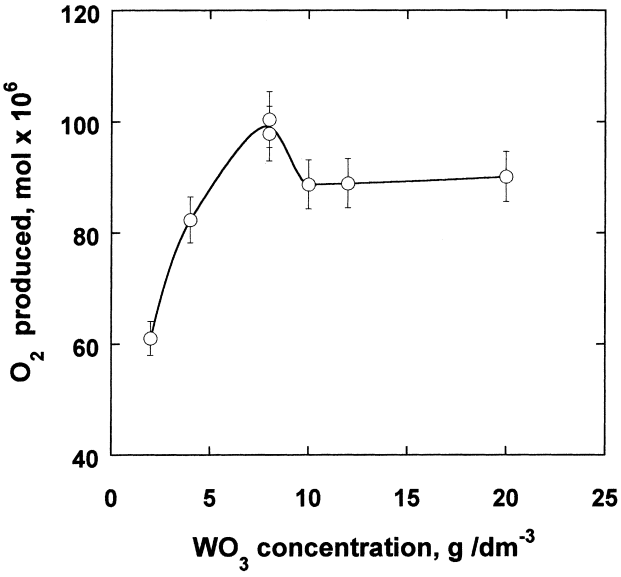

Fig. 4. Dependence of O_2 yield on the amount of WO_3 in the dispersion. Irradiation time = 20 h; $[Fe^{3+}] = 4 \times 10^{-3}$ mol dm^{-3}; pH = 2.4; $\lambda_i \geq 420$ nm; $T = 311$ K.

priate light filters, and the results are summarized in Table 2 (entries 1 to 4). It is apparent that only the light with wavelength below 500 nm was efficient for both WO_3 band gap irradiation and the evolution of O_2. Under illumination with light of wavelengths $\lambda_i \geq 300$ nm, O_2 evolution was much higher than in the case of $\lambda_i \geq 420$. Only tiny O_2 yields were noted when the suspension was exposed to the light in the long-wavelength region ($\lambda_i \geq 620$ nm), indicating that longer wavelength lines are beyond the energy barrier for WO_3. In other words, the WO_3–H_2O–Fe^{3+} dispersion is transparent to light at $\lambda_i > 620$ nm. Although not addressed in this study, the yield of O_2 might also depend on the irradiation intensity and the light quanta absorbed by the suspension. This will be a subject of a separate investigation.

Table 2 also lists the dependence of O_2 production on the ligand in the ferric salt (entries 5–7). Although not shown, the O_2 evolution profiles from the other salts were nearly the same as that of $Fe_2(SO_4)_3$. It is noticeable from Table 2 that dispersions containing $Fe(NO_3)_3$ gave O_2 at an initial rate about two times higher than that of $Fe_2(SO_4)_3$ but the long term yield was slightly lower than that from $Fe_2(SO_4)_3$ dispersions. This is probably due to the photocatalytic conversion of nitrate ions to ammonia at long illumination times [42]. A slightly higher initial rate of O_2 evolution was observed when $Fe_2(SO_4)_3$ was replaced by $FeCl_3$ but O_2 production from the suspension containing $FeCl_3$ deteriorated at longer illumination periods. Among the various possible reasons, one is that the potential for oxygen evolution is close to that for Cl^- oxidation. Since the band edges of WO_3 encompass both the H_2O/O_2 and Cl^-/Cl_2 redox levels, there may be some competition for holes photogenerated in the WO_3 valence band between the oxidation of water to form oxygen and the oxidation of chloride ions to form chlorine. No attempts were made to analyze chlorine. We chose $Fe_2(SO_4)_3$ for further experiments so as to avoid undesired side reactions that occur with other examined salts, such as the partial decomposition of aqueous NO_3^- to nitrogen oxides and oxygen under UV irradiation, and because the water solutions of ferric sulfate are more stable than those of other iron (III) salts.

3.2.5. *Oxygen production from the annular photoreactor*

The time dependence of the evolution of oxygen in the annular photoreactor is shown in Fig. 5. As seen, O_2 production first increases steeply, almost linearly with time, until it reaches a stationary state after 5 h of irradiation. The maximum quantity of oxygen obtained was 410–420 μmol. Such a sharp rise and quick leveling off of product yields is typical of annular batch systems. In most cases, it is found that pumping to remove gas products at the end of the run and re-irradiation, more or less restores the original activity [10,14,16]. It can also be seen in Fig. 5 that the initial rate of O_2 generation varied with the amount of WO_3 and $Fe_2(SO_4)_3$ used. A comparison of O_2 evolution results in Fig. 2 and Fig. 5 reveals that for comparable concentrations of WO_3

Table 2
The production of O_2 from 100 cm^{-3} WO_3 suspensions under various conditions and the influence of used ferric (III) salt in an outer-irradiation cell. 8 g dm^{-3} WO_3 powder is contained in a stirred aqueous suspension containing Fe^{3+} ions under argon

Suspension	λ_i (nm)	$[Fe^{3+}]_0$ (mM)	pH	$r^0_{O_2}$ [a] (μmol h^{-1})	$n_{O_2,20}$ [b] (μmol)
1 WO_3–$Fe_2(SO_4)_3$	≥640	4	2.4	0.4	6
2	≥520			0.7	11
3	≥420			13.1	97
4	≥300			26.3	96
5 WO_3–$FeCl_3$	≥420	4	2.6	18.2	65
6 WO_3–$Fe(NO_3)_3$		4	2.5	31.9	90
7 WO_3–$Fe_2(SO_4)_3$ [c]		4	2.4	13.1	97

[a] $r^0_{O_2}$ refers to the mean initial rate of O_2 evolution which is based on the initial slopes of yields obtained within the first 2 h of irradiation where linearity was maintained.
[b] $n_{O_2,20}$ is the long term yield of O_2, i.e., the total number of moles of O_2 produced after 20 h of irradiation. The reproducibility was within 5%.
[c] Data for this suspension is an average of three repeat runs.

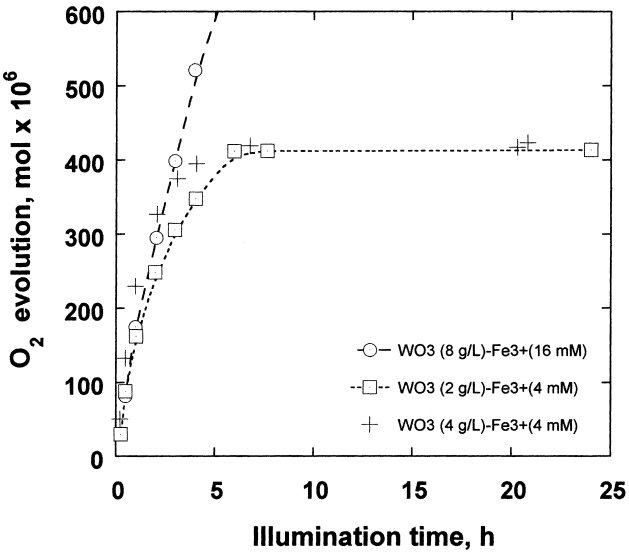

Fig. 5. Activity of WO_3 for O_2 evolution as a function of irradiation time in a 1.1 dm^{-3} annular photoreactor. Conditions: Light source, 400 W Hg lamp; $\lambda_i \geq 300$ nm; T, 300 K.

and Fe^{3+}, the mean O_2 formation rate in an annular reactor ($r_{O_2} = 160\,\mu mol\,h^{-1}$) is about ten times higher than that obtained from the outer-irradiation cell ($r_{O_2} = 13\,\mu mol\,h^{-1}$). This can be mainly attributed to high energy photons generated from the inner-irradiation lamp, and differences in mixing characteristics. Other additional differences include reflection losses, and radiation extinction by the catalyst, i.e., low and medium to high levels of irradiation coexisting in different regions of the photoreactor. The latter effect was particularly noticeable in the outer-irradiation system when colored light was used.

3.3. Simultaneous production of oxygen and hydrogen

Illumination and absorption of ultra-violet light of wavelength 200–300 nm is necessary for the photoexcitation of Fe^{2+} and evolution of hydrogen from aqueous solutions. Thus for experiments in which simultaneous hydrogen and oxygen evolution was desired, we resorted to the annular photoreactor which generated appropriate wavelengths.

Irradiation of a 0.7 mM $FeSO_4$ + 0.03 M H_2SO_4 solution alone led to the production of only H_2 at a rate of 7 $\mu mol\,h^{-1}$, whereas illumination of an aqueous dispersion of WO_3–$Fe_2(SO_4)_3$–$FeSO_4$ in 0.03–0.1 M H_2SO_4 resulted in the appreciable evolution of O_2 accompanied with H_2, as shown in Fig. 6(a). A notable feature of Fig. 6(a) is that a minimal induction period of a few minutes was usually observed followed by an approximate linear growth of H_2 and O_2.

Fig. 6(b) shows that H_2 yield showed a marked dependence on the H^+ ion concentration. The yield increased with decreasing pH. By contrast, the effect of pH was opposite for O_2 production.

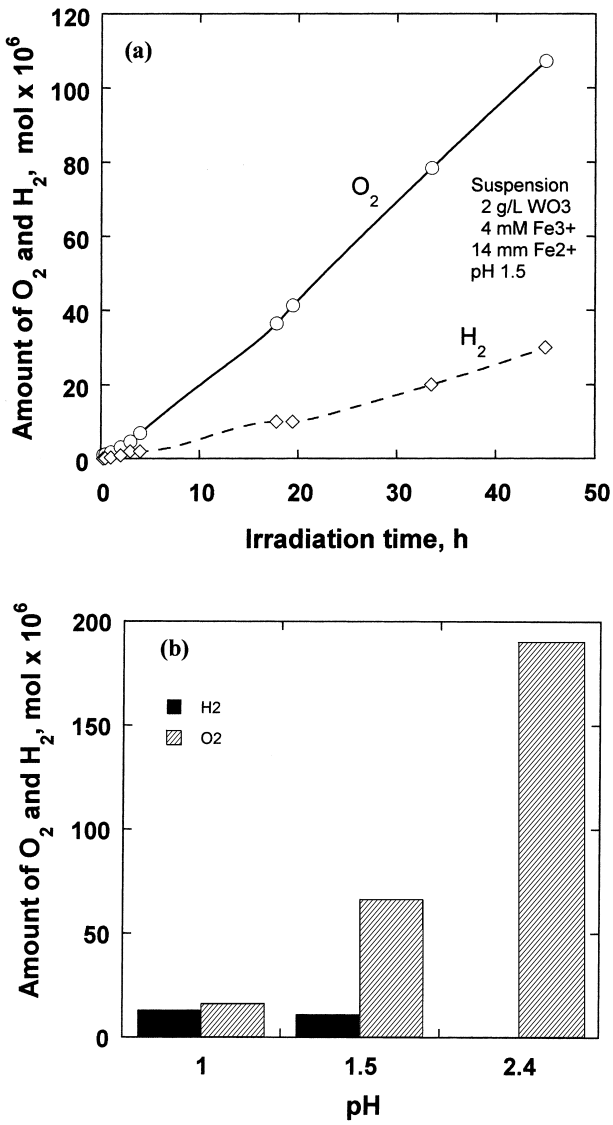

Fig. 6. Time course of H_2 and O_2 production (a) and pH dependence of the yield of H_2 and O_2 (b) produced by the irradiation of a 350 cm^{-3} aqueous suspension containing 0.8 g WO_3, 4 mM Fe^{3+} and 8–16 mM Fe^{2+} species. Conditions: annular reactor; $\lambda_i \geq 200$ nm; T, 300 K.

4. Discussion

4.1. Effect of selected reaction parameters

The present study has established several basic features concerning the performance of the WO_3–H_2O–Fe^{3+}–Fe^{2+} system for the simultaneous photoproduction of H_2 and O_2. Although it is difficult to compare the above data with those reported in the literature due to differences in configurations, irradiation sources and reactor geometry, temperature, among others, the product yields obtained here compare well with those reported previously [3–16,26–30]. The following is an attempt to rationalize the results presented in the preceding section.

4.1.1. Dependence of O_2 yield on illumination time

From the time dependence data displayed in Figs. 2 and 5, it can be seen that WO_3 exhibits good photostability but the rate of O_2 evolution decreases with prolonged illumination. The fall in the O_2 production rate with time can be ascribed to the gradual transformation of Fe^{3+} into Fe^{2+}, and the subsequent depletion of Fe^{3+} as the reaction progresses. This is clearly shown in spectrum (f) of Fig. 1(b) where lack of Fe^{3+} ions at the end of the experiment with WO_3 (4 g dm^{-3})–Fe^{3+} (4 mM) is indicated by the absence of significant absorption in the region between 300 and 380 nm. The lack of adequately fast replenishment of Fe^{3+} ions will negatively affect the rate of interaction between the photogenerated electrons and Fe^{3+} ions, and as a consequence, increase the probability of the deleterious electron-hole recombination. This, in turn, will eventually lead to the fall in the rate of water oxidation to O_2. Other possible reasons may be the equilibrium limitations, i.e., reversal of Eq. (11) as the concentration of Fe^{2+} grows, and the buildup of oxygen partial pressure in the gas phase at extended illumination periods. One should also take into account the fact that, as the concentration of Fe^{2+} grows, some of the photoproduced and dissolved oxygen may be consumed in a slow Fe^{2+} oxidation process that takes place in oxygen-rich aqueous acidic solutions.

4.1.2. Dependence of O_2 production on pH

As to the effect of pH, it is inferred that, to photocatalytically produce O_2 using Fe^{3+} species as an electron acceptor, the pH window in which one can operate is very narrow and is limited to pH < 3. At pH > 3.5, Fe^{3+} ions undergo complete precipitation into a red-brown, light absorbing $Fe(OH)_3$ ($pK_s = 37.4$). Lowering the pH results in the shift of the redox potential of the Fe^{2+}/Fe^{3+} couple. For example, $E^0_{Fe^{2+}/Fe^{3+}}$ falls from +0.77 V at pH 7 to +0.53 V versus NHE at pH 0 [31]. Although the change is relatively small, the shift of $E^0_{Fe^{2+}/Fe^{3+}}$ in the negative direction may negatively influence the reactions in Eqs. (7)–(11) presented further in the text. This is so because this shift will result in a fall in the driving force for the reduction of Fe^{3+} ions to Fe^{2+}. We would be remiss not to mention the influence of the addition of foreign ions such as H^+, $SO_4{}^{2-}$ and Na^+ during pH adjustment. Addition of foreign ions may modify the properties of the suspension, such as, the ionic strength, shift of WO_3 flatband potential, the adsorption and coordination of ions in the solution onto WO_3 particles, and the resulting charge compensation. For example, at pH values more acidic than the point of zero charge, WO_3 particles can undergo the normal charging process, i.e., they can easily associate protons from the solution phase and acquire positive charge. A considerable change in any of these properties is likely to affect the inter-phase charge transfer at the WO_3 particle/solution interface, and consequently, the intrinsic kinetics of O_2 production during long term irradiation. The effects of these factors are beyond the scope of the present investigation. Another noticeable thing was that in suspensions with pH < 2, agglomeration of some of the WO_3 particles occurred on the Teflon magnetic stirring bar at extended illumination periods. It is known that tungsten oxide hydrate polymerizes into isopolytungstates in strongly acidic solutions [23]. Perhaps this is what was observed on the stirring bar. No attempt was undertaken to verify the formation of such polymerized products.

4.1.3. Dependence on Fe^{3+} initial concentration

The activity enhancement observed with increasing Fe^{3+} concentration in the examined range may be partly explained by the fact that a gradual rise in Fe^{3+} concentration will lead to higher interfacial concentrations of Fe^{3+} species, which would subsequently result in the increased access to a large population of Fe^{3+} ions in the vicinity of the WO_3 particle surface. This, in turn, will increase the probability of interaction between photogenerated electrons and Fe^{3+} species, thus improving the overall electron-hole pair dissociation and charge separation, and as a result favoring the oxygen evolution process. Also, a sufficiently large population of Fe^{3+} species in the proximity of a WO_3 particulate may create a suitable electric field which can lead to Fe^{3+} cations acting as surface states that can trap photogenerated electrons. This may help the e^-–h^+ charge separation, as indicated in Eq. (5). The decline in O_2 yield at high Fe^{3+} concentrations can be attributed, among other things, (i) to the aqueous chemistry considerations described briefly in the preceding paragraph, (ii) to the change in the net surface charge, and potential distribution across the inter-phase layer and (iii) to inter-phase diffusion limitations, for example, the transport of Fe^{3+} to the close proximity of a WO_3 particle, and the ability of produced Fe^{2+} ions to migrate away into solution.

4.1.4. Dependence on the amount of WO_3

The variation in O_2 evolution with WO_3 content may be rationalized as follows. The maximum attained at 8 g dm^{-3} WO_3 indicates that such a concentration of WO_3 particles in the suspension ensures maximum light absorption. The descending portion observed at $C_{WO_3} > 8$ g dm^{-3} is attributed to the drop in the number of incident photons reaching the bulk of the suspension due to the shadowing effect of WO_3 particles, thus reducing the number of electrons and holes available for the reaction, and consequently, reducing O_2 production. Another reason for the observed decrease in O_2 yield might be the agglomeration effect of the collisions between WO_3 particles at higher WO_3 concentrations. The independence of O_2 yield at $C_{WO_3} > 8$ g dm^{-3} could be suggestive of the saturation of the suspension by photons.

4.1.5. Simultaneous production of oxygen and hydrogen

The data in Fig. 6 show that reasonable evolution of O_2 and H_2 can be produced simultaneously from the studied system. From the obtained results, it is noticeable that O_2 and H_2 yields are undoubtedly small in comparison with those obtained when these gases are produced separately.

Apart from the possible back reaction of hydrogen and oxygen, this is due to a combination of disconcerting reaction characteristics for the production of O_2 and H_2. For instance, both O_2 and H_2 showed a marked dependence on the proton concentration but in different ways. Low pH implies higher concentrations of H^+ ions, and therefore, higher yields of H_2. The same applies for initial $FeSO_4$ concentration (see reactions 12–15). Conversely, high concentrations of H^+ inhibit O_2 production since O_2 evolution is accompanied by the release of protons, as is evident in Fig. 6(b), and in Eq. (8) and Eq. (11). Thus for a given system, a compromise with respect to these variables and a proper choice of operating conditions have to be made. The present system is at an early stage and improved yields can be obtained, for example, by modifying WO_3 with dopants, and choosing an appropriate redox couple and suitable proportions of contents in the suspension. The results from such a study will be presented in a subsequent paper of this series.

4.2. Reaction scheme for the production of O_2 and H_2

4.2.1. Photocatalytic production of O_2

The reaction scheme for the production of O_2 can be envisioned as follows. The reaction is initiated when light energy larger than the WO_3 band gap ($E_{BG}^{WO_3} \geq 2.6$ eV) is absorbed by the WO_3 particles forming an electron (e^-) and hole (h^+) pair in the semiconductor as described in Eq. (3). The deleterious recombination of electrons and holes in the lattice (see Eq. (4)) can be avoided if the two species are separated, and subsequently, trapped by appropriate sites on the WO_3 surface defects, e.g., electrons on W^{6+} in WO_3 [32,33], or transferred to species bound to the surface, as illustrated in Eqs. (5)–(7).

$$WO_3 + h\nu \rightarrow e^-_{CB} + h^+_{VB} \quad (3)$$

$$e^-_{CB} + h^+_{VB} \rightarrow \text{recombination} \rightarrow \text{heat} \quad (4)$$

$$e^-_{CB} \rightarrow e^-_{tr} \quad (5)$$

$$h^+_{VB} \rightarrow h^+_{tr} \quad (6)$$

The subscripts CB and VB denote conduction and valence band, respectively.

Following photoexcitation and trapping of charges, surface-adsorbed Fe^{3+} scavenges away the trapped electrons at the interface, forming its reduced state Fe^{2+} according to the reaction (7) [26,27]. The electron transfer from a WO_3 particle conduction band into the Fe^{3+} $3d^5$ orbital is energetically favored because the flatband potential of WO_3 is more negative than the standard electrochemical potential of the Fe^{3+}/Fe^{2+} couple ($E^0_{Fe^{3+}/Fe^{2+}} = +0.71$ V versus NHE in acidic conditions $[H^+] = 0.5$ M).

$$e^-_{tr} + Fe^{3+}_{aq} \rightarrow Fe^{2+}_{aq} \quad (7)$$

Simultaneously, the trapped holes in the reaction (6) oxidize water molecules in a four-electron exchange process to give oxygen as expressed in the reaction (8):

$$4h^+_{tr} + 2H_2O \rightarrow 4H^+_{aq} + O_{2(gas)} \quad (8)$$

Other probable parallel pathways that are necessary to consider are (i) the possible reduction of the produced but still adsorbed oxygen by e^-_{tr} to generate O_2^- or equivalent species and (ii) the interaction of h^+_{tr} with Fe^+_{aq}.

$$O_{2(ads)} + e^-_{tr} \rightarrow O_{2(ads)}^- \quad (9)$$

$$Fe^{2+}_{aq} + h^+_{tr} \rightarrow Fe^{3+}_{aq} \quad (10)$$

The net process for O_2 production from this system can be summarized as

$$4Fe^{3+}_{aq} + 2H_2O \xrightarrow[WO_3]{h\nu} 4Fe^{2+}_{aq} + 2H^+ + O_{2(gas)} \quad (11)$$

4.2.2. Photochemical production of hydrogen

In this work, hydrogen production was achieved by irradiation of the suspension with light of $\lambda_i \geq 200$ nm. Ultraviolet irradiation of the suspension containing Fe^{3+}_{aq} produces the excited state $^*Fe^{2+}_{aq}$, which then decays to give rise to Fe^{3+}_{aq} species and a solvated electron, e^-_{aq} in the primary photoprocess according to the following reaction scheme [34–38]:

$$Fe^{2+}_{aq} \xrightarrow[\lambda_i < 300\,nm]{h\nu} {}^*Fe^{2+}_{aq} \quad (12)$$

$$^*Fe^{2+}_{aq} \xrightarrow[H_2O]{} [^*Fe^{3+} - H_2O^-] \rightarrow Fe^{3+}_{aq} + e^-_{aq} + H_2O \quad (13)$$

The reaction of the hydrated electron with H^+ (H_3O^+) yields a hydrogen radical $H^\bullet$, and the subsequent combination of hydrogen radicals leads to the evolution of dihydrogen into the gas phase via the general reactions (14) and (15).

$$e^-_{aq} + H^+_{aq} \rightarrow H^\bullet_{aq} \quad (14)$$

$$2H^\bullet_{aq} \rightarrow H_{2aq} \rightarrow H_{2(gas)} \quad (15)$$

A possible alternative side reaction is the back reaction

$$Fe^{3+}_{aq} + H^\bullet_{aq} = Fe^{2+}_{aq} + H^+_{aq} \quad (16)$$

where the subscripts aq and gas denote aqueous and gas phase, respectively.

It is apparent from the above scheme that reactions (11) and (13) complete a $Fe^{3+}_{aq} - Fe^{2+}_{aq}$ cycle which can be repeated many times as the reaction progresses.

In summary, the sum of reactions (3) to (15) is equivalent to photodecomposition of H_2O into O_2 and H_2.

5. Conclusions

This study has demonstrated that, under illumination, a properly selected semiconductor particulate system and a suitably matched redox couple can give modest yields of O_2 and H_2, and that these yields can be sustained over long illumination periods. The obtained results have demon-

strated that aqueous WO_3–Fe^{2+}/Fe^{3+} dispersions are stable and active towards O_2 and H_2 production under a variety of operating conditions. The production of O_2 and H_2 was found to be sensitive to illumination time and wavelength, initial concentration of Fe^{3+} and Fe^{2+} cations, concentration of WO_3, and pH.

The overall reaction scheme for the production of O_2 and H_2 from the photodecomposition of water is a two-step photoexcitation process in which the photocatalytic evolution of O_2 involves the oxidation of water by holes generated from the excitation of WO_3 particles. Hydrogen production proceeds via the light-driven photochemical excitation of Fe^{2+}_{aq} species in the solution phase of the suspension.

Although the WO_3–Fe^{2+}/Fe^{3+}–$h\nu$ system works well in acidic media, the main limitation of using a Fe^{2+}/Fe^{3+} redox couple is that photocatalysts which can be used for O_2 evolution are limited to materials that are stable against corrosion and dissolution in acidic aqueous solutions. Another constraint is the limited pH window of this system. At pH > 3.5, Fe^{3+} ions undergo complete precipitation into red-brown, light absorbing $Fe(OH)_3$. Nonetheless, the data obtained in this work strongly suggest that the studied system has some potential for the efficient and combined photoproduction of oxygen and hydrogen by splitting water.

Further studies are in progress in order to develop materials by the controlled modification of WO_3 so as to get materials with appropriate band edges to effect the photodecomposition of water using a significant part of the visible region of the solar spectrum.

References

[1] M. Shiavello (Ed.), Photochemistry, Photocatalysis, and Photoreactors; Mathematical and Physical Sciences, vol. 146, Reidel, Dordrecht, 1984.
[2] M. Chanon (Ed.), Homegeneous Photocatalysis; Photoscience and Photoengineering Series, vol. 2, Wiley, New York, USA, 1997.
[3] K. Yamaguchi, S. Sato, J. Chem. Soc., Faraday Trans. 1 81 (1985) 1237.
[4] K. Domen, A. Kudo, T. Onishi, J. Catalysis 102 (1986) 92.
[5] Y. Inoue, T. Kubokawa, K. Sato, Chem. Commun. (1990) 1298.
[6] Y. Inoue, T. Kubokawa, K. Sato, J. Phys. Chem. 95 (1991) 4059.
[7] Y. Inoue, T. Niiyama, Y. Asai, K. Sato, Chem. Commun. (1992) 579.
[8] M. Kohno, T. Kaneko, Y. Inoue, J. Chem. Soc., Faraday Trans. 1 94 (1998) 89.
[9] K. Sayama, H. Arakawa, J. Phys. Chem. 97 (1993) 531.
[10] K. Sayama, H. Arakawa, J. Photochem. Photobiol. A: Chem. 77 (1994) 243.
[11] A. Tanaka, A. Tanaka, K. Shinohara, M. Hara, J.N. Kondo, K. Domen, Chem. Mater. 9 (1997) 1063.
[12] A. Kudo, H. Kato, Chem. Lett. 9 (1997) 867.
[13] M. Hara, T. Kondo, M. Komoda, S. Ikeda, K. Shinohara, A. Tanaka, K. Domen, Chem. Commun. 3 (1998) 357.
[14] K. Sayama, K. Yase, H. Arakawa, K. Asakura, A. Tanaka, K. Domen, T. Onishi, J. Photochem. Photobiol. A: Chem. 114 (1998) 125.
[15] K.H. Chung, D.C. Park, J. Mol. Catalysis 129 (1998) 53.
[16] K. Sayama, R. Yoshida, H. Kusama, K. Okabe, Y. Abe, H. Arakawa, Chem. Phys. Lett. 277 (1997) 387.
[17] S. Swada, G.C. Danielson, Phys. Rev. 113 (1959) 1008.
[18] D.E. Scaife, Solar Energy 25 (1980) 41.
[19] W. Erbs, J. Desilvestro, E. Borgarello, M. Gratzel, J. Phys. Chem. 88 (1984) 4001.
[20] J. Desilvestro, M. Neumann-Spallart, J. Phys. Chem. 89 (1985) 3684.
[21] S.A. Stevenson (Ed.), Metal-Support Interactions in Catalysis, Sintering and Redispersion, van Nostrand, New York, USA, 1987.
[22] K. Tanabe, M. Misono, Y. Ono, H. Hattori (Eds.), Studies in Surface Science and Catalysis, Elsevier, Amsterdam, Holland, 51 (1989) 21.
[23] B. Elvers, S. Hawkins (Eds.), Ullmann's Encyclopedia of Industrial Chemistry, vol. A27, VCH Publ., Weinheim, Germany, 1996, p. 256.
[24] H. Demiryont, K.E. Nietering, Appl. Opt. 28 (1989) 1494.
[25] H.J.H. Fenton, J. Chem. Soc. 65 (1894) 899.
[26] A.A. Kranovskii, G.P. Brin, Dokl. Akad. Nauk. SSR 147 (1962) 656.
[27] A.A. Kranovskii, G.V. Fomin, G.P. Brin, M.V. Genkin, A.K. Lynbimova, L.A. Blyamenfel'd, Dokl. Akad. Nauk. SSR 212 (1973) 424.
[28] J.R. Darwent, A. Mills, J. Chem. Soc., Faraday Trans. 2 78 (1978) 359.
[29] M.D. Ward, A.J. Bard, J. Phys. Chem. 86 (1982) 3599.
[30] T. Ohno, D. Haga, K. Fujihara, K. Kaizaki, M. Matsumura, J. Phys. Chem. B 101 (1997) 6415.
[31] A.J. Bethume, N.A.S. Loud (Eds.), Standard Aqueous Electrode Potentials and Temperature Coefficients at 25°C, Clifford A. Hempel, London, UK, 1964.
[32] M.T. Nenadovich, T. Rajh, O.I. Micic, A.J. Nozik, J. Phys. Chem. 88 (1984) 5827.
[33] G.V. Buxton, C.L. Greenstock, W.P. Helman, A.B. Ross, J. Phys. Chem. Ref. Data 17 (1988) 513.
[34] T. Rigg, G. Stein, J. Weiss, Proc. R. Soc. A 211 (1952) 375.
[35] T. Rigg, J. Weiss, J. Chem. Phys. 20 (1952) 1194.
[36] F.S. Dainton, F.T. Jones, Trans. Faraday Soc. 61 (1965) 1681.
[37] P.L. Airey, F.S. Dainton, Proc. R. Soc. London A 291 (1966) 340.
[38] P.S. Bratermann, A.G. Cairns-Smith, R.W. Sloper, T.G. Truscott, M.J. Craw, J. Chem. Soc., Dalton Trans. 7 (1984) 1441 and references therein.
[39] H.P. Maruska, A.K. Ghosh, Solar Energy 20 (1978) 445.
[40] S.R. Morrison (Ed.), Electrochemistry at Semiconductor and Oxidized Metal Electrodes, Plenum Press, New York, London, 1980.
[41] G. Hodes, E.A. Klaus, B.P. Gunn, J.R. Locker, W.E. Serafin, S. Srinivasan, Electrochim. Acta 23 (1978) 521.
[42] B.J. Liu, T. Torimoto, H. Yoneyama, J. Photochem. Photobiol. A: Chem. 115 (1998) 227.